ARTICLE OPEN

Check for updates

Polyploid cancer cells reveal signatures of chemotherapy resistance

Michael J. Schmidt[1,9], Amin Naghdloo[1], Rishvanth K. Prabakar[1,10], Mohamed Kamal[1,2], Radu Cadaneanu[3], Isla P. Garraway[3], Michael Lewis[4,5,6], Ana Aparicio[7], Amado Zurita-Saavedra[7], Paul Corn[7], Peter Kuhn[1], Kenneth J. Pienta[8], Sarah R. Amend[8]✉ and James Hicks[1]✉

Therapeutic resistance in cancer significantly contributes to mortality, with many patients eventually experiencing recurrence after initial treatment responses. Recent studies have identified therapy-resistant large polyploid cancer cells in patient tissues, particularly in late-stage prostate cancer, linking them to advanced disease and relapse. Here, we analyzed bone marrow aspirates from 44 advanced prostate cancer patients and found the presence of circulating tumor cells with increased genomic content (CTC-IGC) was significantly associated with poorer progression-free survival. Single cell copy number profiling of CTC-IGC displayed clonal origins with typical CTCs, suggesting complete polyploidization. Induced polyploid cancer cells from PC3 and MDA-MB-231 cell lines treated with docetaxel or cisplatin were examined through single cell DNA sequencing, RNA sequencing, and protein immunofluorescence. Novel RNA and protein markers, including HOMER1, TNFRSF9, and LRP1, were identified as linked to chemotherapy resistance. These markers were also present in a subset of patient CTCs and are associated with recurrence in public gene expression data. This study highlights the prognostic significance of large polyploid tumor cells, their role in chemotherapy resistance, and the expression of markers tied to cancer relapse, offering new potential avenues for therapeutic development.

Oncogene; https://doi.org/10.1038/s41388-024-03212-z

INTRODUCTION

While initial treatment efficacy is observed in most patients with prostate or breast cancer, prostate cancers recur in 24-48% of cases [1], and breast cancers relapse in about 30% of patients [2, 3]. In general, late-stage metastatic cancers are more difficult to control, and patients are typically treated with chemotherapy; unfortunately, complete response rates from chemotherapy treatments in patients with late stage disease are low [4, 5]. Despite defining numerous detailed intrinsic and extrinsic mechanisms that enable cancer cell survival under therapy, therapy resistance remains responsible for over 90% of cancer related deaths [6–8].

Large polyploid tumor cells are correlated with late disease stages, poor prognosis, and therapy resistance across virtually every tumor type [9–13]. Large polyploid tumor cells are induced through various stressors, including common chemotherapies such as docetaxel and cisplatin [14–17]. Evidence has shown that whole genome doubling (WGD) events and altered ploidy levels are poor prognostic indicators across cancer types and are ultimately thought to provide cancer cells the ability to evolve and survive therapy [18–21].

Recent studies have shown that large polyploid tumor cells can give rise to viable progeny that display more malignant and stem cell characteristics than the parental population they descended from [22]. Importantly, targeting identified pathways, including AP-1, HIF2α, cholesterol-related, and embryogenic-related pathways, reduced the number of surviving large polyploid cancer cells, as well as surviving progeny cells following therapy [22–26]. While significant, these studies lack single-cell molecular resolution and note that not all cells are eliminated. What ultimately matters is that some cancer cells are still capable of survival and result in disease progression. Identification of novel biomarkers that can predict patients' recurrence and resistance to therapy may lead to better treatment outcomes.

We find that the presence of circulating tumor cells with increased genomic content (CTC-IGC) in the bone marrow aspirate of late-stage prostate cancer patients is significantly associated with worse progression free survival. We comprehensively evaluated large polyploid tumor cells (prostate cancer PC3 and breast cancer MDA-MB-231) that survive following treatment with two chemotherapy classes (cisplatin and docetaxel), and functionally characterize the surviving cells through a multi-omic approach, including morphometric, genomic, and transcriptomic profiling at the single cell level. We find that progeny cells differed substantially from the original parental population and most

[1]Convergent Science Institute in Cancer, Michelson Center for Convergent Bioscience, University of Southern California, Los Angeles, CA, USA. [2]Department of Zoology, Faculty of Science, Benha University, Benha, Egypt. [3]Department of Urology, Jonsson Comprehensive Cancer Center, David Geffen School of Medicine at UCLA and VA Greater Los Angeles, University of California, Los Angeles, Los Angeles, CA, USA. [4]VA Greater Los Angeles Medical Center, Los Angeles, CA, USA. [5]Departments of Medicine and Pathology, Cedars-Sinai Medical Center, Los Angeles, CA, USA. [6]Center for Cancer Research and Cellular Therapeutics, Clark, Atlanta, GA, USA. [7]Department of Genitourinary Medical Oncology, The University of Texas MD Anderson Cancer Center, Houston, TX, USA. [8]Cancer Ecology Center, The Brady Urological Institute, Johns Hopkins University School of Medicine, Baltimore, MD, USA. [9]Present address: Department of Pediatric Oncology, Dana-Farber Cancer Institute, Boston, MA, USA. [10]Present address: Simons Center for Quantitative Biology, Cold Spring Harbor Laboratory, Cold Spring Harbor, NY, USA. ✉email: samend2@jhmi.edu; jameshic@usc.edu

Received: 15 August 2024 Revised: 24 October 2024 Accepted: 28 October 2024
Published online: 22 November 2024

closely resembled the transcriptome of the large polyploid tumor cells from which they were derived. We also find novel markers associated with chemotherapy survival are upregulated in cells that survive treatment, are retained in the progeny from surviving cells, and are significantly associated with recurrence in prostate and breast cancer at the RNA level. These novel survival biomarkers are expressed at the protein level in the CTCs of patients who also have recurrent disease. Taken together, our results highlight novel biomarkers of survival and shed light on the functionality of large polyploid tumor cells and their role in disease recurrence.

RESULTS

CTCs with increased genomic content (CTC-IGC) are found in the bone marrow aspirate of late-stage prostate cancer patients and are correlated with worse progression free survival

Liquid biopsies from peripheral blood and bone marrow aspirate were acquired from a late-stage prostate cancer cohort (NCT01505868). Matched bone marrow and peripheral blood samples from 31 patients were analyzed for CTCs. CTC-IGC, identified as having a nuclear diameter at least double the average of the CTC cell population, were found in 9.7% of peripheral blood samples. CTC-IGC were present in 80.6% of bone marrow samples from the same patients (Fig. 1A, B, S1). Survival analysis with 44 bone marrow samples (from the 31 patients with matched blood samples and 13 patients without matched blood) showed that the presence of at least one CTC-IGC detected in the bone marrow was associated with decreased progression-free survival (Fig. 1C, Table S1). Previous treatment history was available for 33 of the 44 patients and primarily included anti-androgens and other hormonal treatments (i.e., bicalutamide, nilutamide, enzalutamide). The six patients who were previously treated with docetaxel were all positive for CTC-IGC in the bone marrow (Table S1).

Clonal tumor lineage measured via copy number ratio analysis was confirmed in both typical CTCs and CTC-IGC. No apparent differences in copy number ratios were identified between the two CTC groups (Figs. 1D–F, S2, S3). Further, copy number concordance analysis showed no statistical differences between typical CTCs and CTC-IGCs; in fact, CTC-IGCs were more concordant with each typical CTCs than other CTC-IGCs (Fig. S4A, Table S2). These observations show that CTC-IGC can be found in blood and bone marrow aspirate, are tumor derived, and thus may contribute towards relapse in late-stage prostate cancer. Despite the apparent WGD of CTC-IGC, these cells retain the original tumor copy number profile. To understand the importance and behavior of this phenotype, we used an in vitro model of polyploid tumor cells to investigate their relationship with therapeutic resistance.

Large polyploid cancer cells form as a response to chemotherapy in prostate and breast cancer models

PC3 and MDA-MB-231 cells were treated with sublethal doses of docetaxel or cisplatin for 72 hours. Following chemotherapy, cells were allowed to recover for 1 or 10 days in their regular growth medium, lifted from culture, plated on Marienfield specialized glass slides, stained with cell and nuclear markers, then imaged through high content scanning and evaluated for nuclear size and

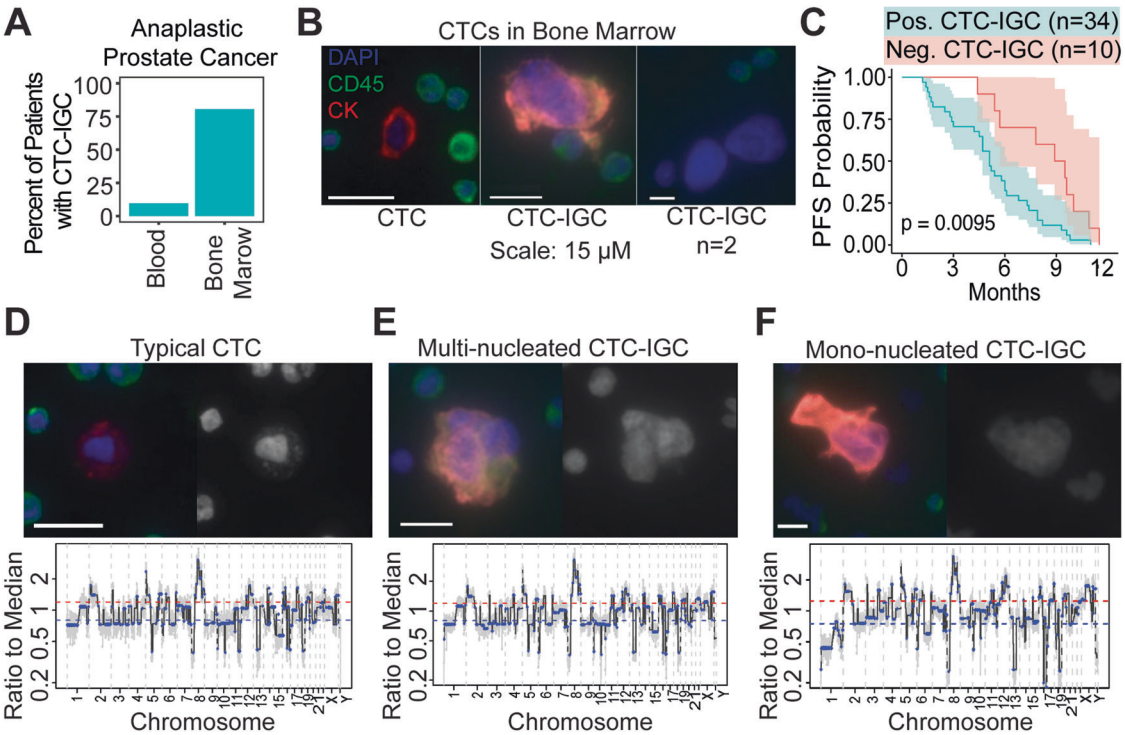

Fig. 1 Large tumor cells are found in bone marrow aspirate of late-stage prostate cancer patients. A Percentage of patients with matched peripheral blood and bone marrow samples with at least 1 CTC-IGC present in liquid biopsy. **B** Representative images of a typical CTC (left) and CTC-IGCs (middle and right) found in bone marrow aspirate. Far right image depicts two ($n = 2$) CTC-IGC cells that are EPI-negative but are confirmed to be tumor derived (see Fig S2A). Scale bars set to 15 μM. **C** PFS from patients with (teal) or without (red) at least one CTC-IGC found in bone marrow samples. **D** Representative image of typical CTC found in bone marrow with merged and DAPI channels (top) and its genomic copy number profile (bottom). **E** Representative image of CTC-IGC found in bone marrow with merged and DAPI images (top) and its genomic copy number profile (bottom). **F** Representative image of mono-nucleated CTC-IGC found in bone marrow with merged (pan-epithelial markers in red, CD45 in green, vimentin in white, and DAPI in blue) and DAPI images (top) and its genomic copy number profile (bottom). Scale bars are set to 15 μM in **D**–**F**.

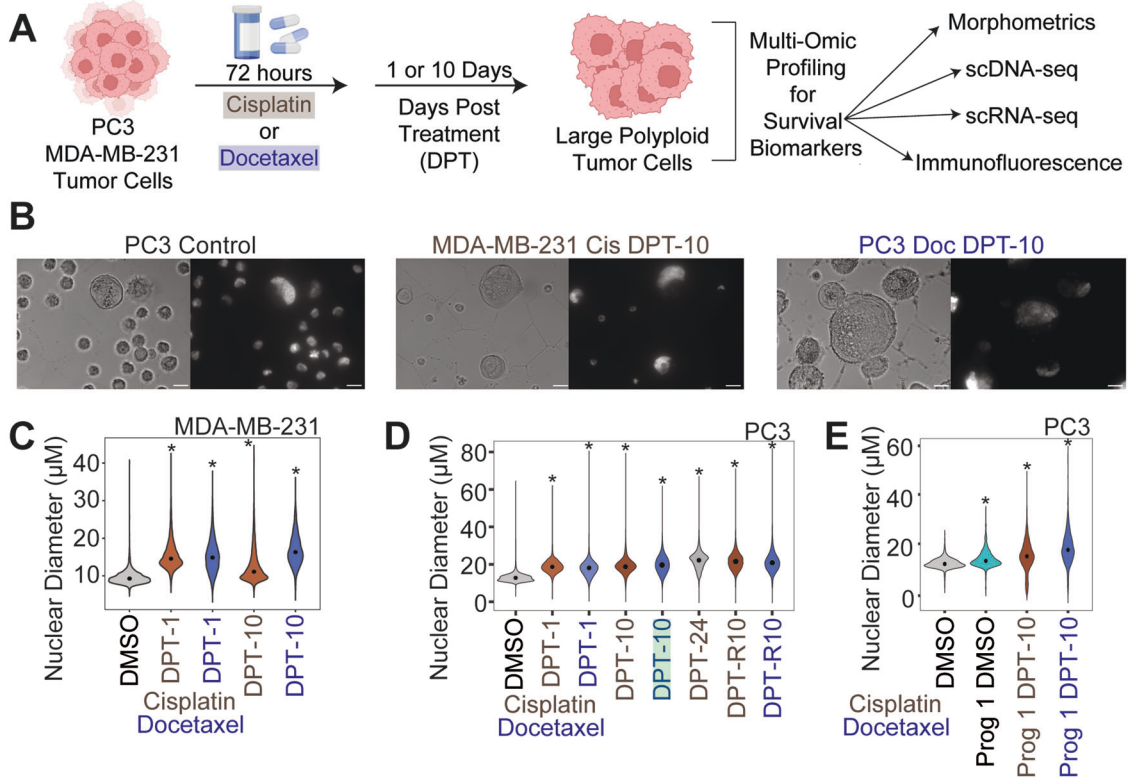

Fig. 2 Large polyploid tumor cells are induced following chemotherapy exposure in MDA-MB-231 and PC3 cell lineages. A Experimental schematic for in vitro investigation of surviving polyploid cells. **B** Representative images in bright field (left) and DAPI (right) channels for PC3 control with a polyploid cell present (left), MDA-MB-231 cisplatin 10 days post treatment (DPT) enriched polyploid (middle), and PC3 docetaxel 10 DPT enriched polyploid (right) conditions. Scale bars are set to 20 μM. **C** Nuclear diameter for MDA-MB-231 control (DMSO), 10 DPT cisplatin, 1 DPT docetaxel, 10 DPT cisplatin, and 10 DPT docetaxel post treatment recovery. **D** Nuclear diameter for PC3 control (DMSO), 1 DPT cisplatin, 1 DPT docetaxel, 10 DPT cisplatin, 10 DPT docetaxel post treatment recovery, 24 DPT cisplatin recovery, 10 DPT cisplatin retreated, and 10 DPT docetaxel retreated. Retreated conditions were initially treated with cisplatin and recovered for 10 days. Teal box on docetaxel DPT 10 indicates the condition where single cell progeny (progeny-1 and progeny-2) originated from. **E** Nuclear diameter of PC3 control parental and progeny-1 cells, and progeny-1 10 DPT recovered cells. All treated conditions in **C**–**E**, and progeny-1 DMSO cells, are significantly larger in nuclear diameter compared to DMSO controls (Wilcoxon rank sum; $p < 0.01$).

other morphometric comparisons (Fig. 2A). While there was significant cell death as expected (Fig. S5A), surviving cells increased in both nuclear diameter and cell size as a function of time (Figs. 2B–E; S5B, S6).

To evaluate resistance, we treated cells that survived cisplatin treatment (10 days post treatment release; 10 DPT) with cisplatin or docetaxel. Compared to the control condition (initially cisplatin treated and then re-treated with DMSO) cell counts and cell viability were not significantly impacted, suggesting that these cells are not sensitive to additional rounds of chemotherapy (Figs. S5A, S5D, 2E).

To obtain progeny cells from a single chemotherapy-induced surviving polyploid cell, we isolated and single-cell seeded PC3 cells 10 days post-cisplatin release ($n = 480$) and 10 days post-docetaxel release ($n = 960$) and monitored for colony formation. From these, only 2 polyploid docetaxel-treated PC3 cells gave rise to progeny after 2 months (progeny-1) and 2.5 months (progeny-2). Progeny-2 failed to proliferate following the first passage. Over the course of the three-month experiment, approximately 50% of the polyploid cells treated with either cisplatin or docetaxel remained viable and adherent. The dividing progeny-1 cells displayed a larger nuclear and cellular diameter than the parental PC3 population from which it originated (Figs. 2E, S5). We treated progeny-1 with docetaxel or cisplatin and found that the population was sensitive to both chemotherapies. Further, following 10 days of recovery, surviving progeny-1 cells had increased nuclear and cell diameter, similar to what was observed from the original parent population (Figs. 2E, S5B).

Surviving PC3 polyploid cancer cells show no additional copy number ratio alterations compared to parental controls

To evaluate the presence of genomic alterations in the surviving polyploid cells and their progeny, we assayed copy number status and cell ploidy. Strikingly, surviving large polyploid PC3 and MDA-MB-231 cells from both docetaxel and cisplatin treatments showed no apparent copy number ratio differences compared to control cells and showed no statistical differences in evaluating copy number concordances (Figs. 3A–C, S4B, S7, Table S3). This result confirms patient data in that copy number ratio status does not differ between CTCs with normal nuclei and CTCs with larger nuclei (Fig. 1D–F) and suggests that cells are undergoing complete WGD rather than displaying specific copy number breakpoints. While copy number status did display minor differences in the progeny-1 compared to parental control (e.g., an increased 3p gain) (Fig. 3A, B), no substantial alterations were observed. Conversely, progeny-2, the clone that did not survive the first passage, displayed the most aberrant copy number profile compared to the other conditions (i.e., 6 gain and 4p gain) and clustered separately from the other PC3 cell conditions (Fig. 3A).

FISH probes for the centromeres of PC3 chromosome 1 (ploidy = 3) and chromosome 10 (ploidy = 1) showed no statistically significant differences when comparing DMSO parental control cells to progeny-1 cells (Fig. 3D), suggesting that any apparent scars of ploidy reduction were not present. These results prompted investigation into the phenotype of these surviving cells.

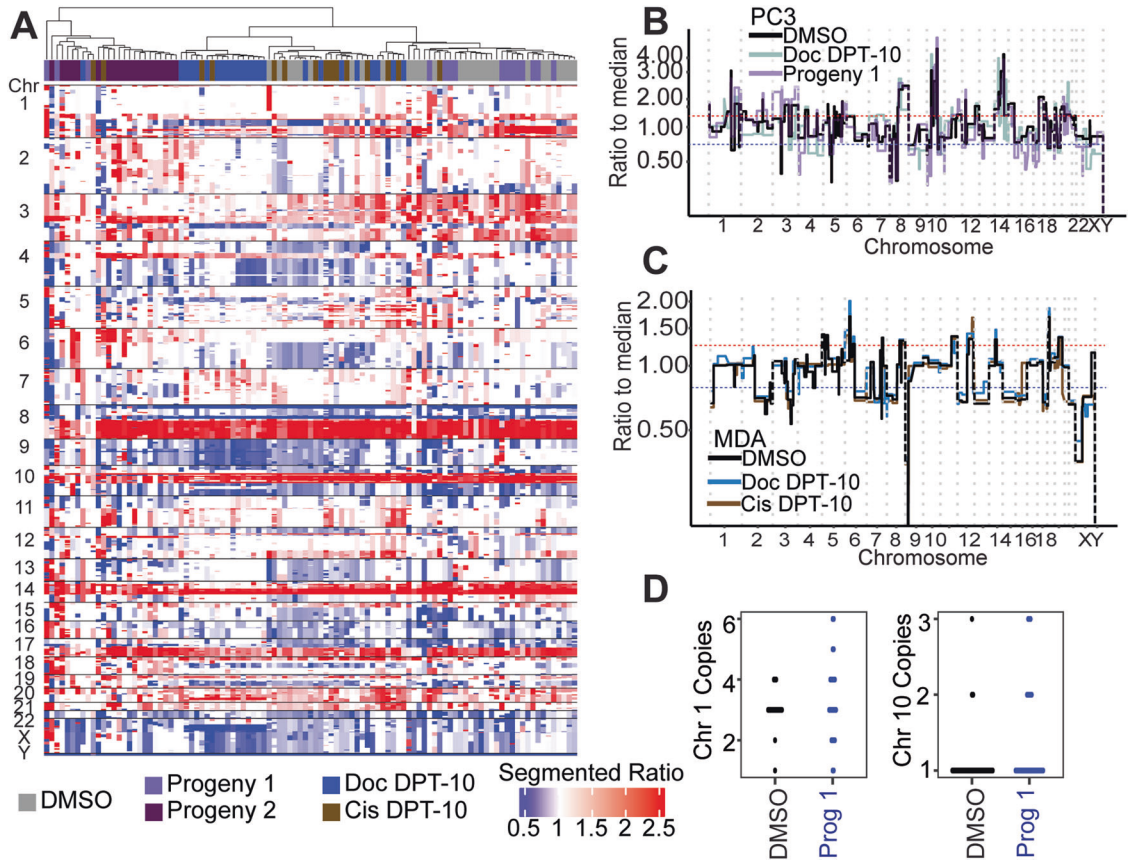

Fig. 3 Single cell genomics of polyploid cell line samples. A Heatmap of segmented copy number ratios for PC3 conditions. Ratio of 1 (white) indicates copy number neutral respective to the entire genome. Left side of heatmap depicts dead and/or dying cells, including progeny-2 cells, which failed to proliferate following first passage. **B** Overlay of representative PC3 DMSO, Doc 10 DPT, and Progeny-1 copy number ratio profiles from cells depicted in **A**. **C** Overlay of representative MDA-MB-231 DMSO control, Doc 10 DPT, and Cis 10 DPT copy number ratio profiles. **D** FISH for PC3 DMSO control and progeny-1 cells for centromere of chromosome 1 (ploidy = 3) and chromosome 10 (ploidy = 1). Each dot represents an individual data point.

Single cell transcriptomic profiling reveals common genes and pathways upregulated in PC3 and MDA-MB-231 polyploid cells

497 PC3 cells were isolated and sequenced in 5 separate batches (Fig. S8) and included: DMSO control ($n = 129$), 1-day post-cisplatin release ($n = 78$), 10 days post-cisplatin release ($n = 68$), 1-day post-docetaxel release ($n = 45$), 10 days post-docetaxel release ($n = 118$), docetaxel progeny-1 ($n = 12$), docetaxel progeny-2 ($n = 13$). Two batches of 203 MDA-MB-231 cells included: DMSO control ($n = 43$), 1-day post-cisplatin release ($n = 22$), 10 days post-cisplatin release ($n = 62$), 1-day post-docetaxel release ($n = 24$), 10 days post-docetaxel release ($n = 62$) (Fig. S9).

Regardless of treatment, a general spatial separation that was dependent on recovery duration was observed in PC3 and MDA-MB-231 cells (Fig. 4A, S10). To identify convergent phenotypes regardless of tumor type or therapy, we evaluated genes that were upregulated in both PC3 and MDA-MB-231 following either cisplatin or docetaxel treatment. MDA-MB-231 cells 10 days post cisplatin or docetaxel release upregulated 1591 shared genes compared to DMSO control; PC3 cells 10 days post cisplatin or docetaxel treatment upregulated 1178 shared genes compared to DMSO control (LFC > 1.5, FDR < 0.01; Fig. 4B). Intersection of the shared gene sets showed MDA-MB-231 and PC3 cells that survive either cisplatin or docetaxel exposure shared 309 upregulated genes (Fig. 4B; Table S4). The 309 shared genes were considered a survivor cell enrichment data set, which was further evaluated.

Of the 309 shared genes, 77% were protein coding and 17% were lncRNAs, while the remaining ~6% were pseudogenes or yet to be experimentally confirmed (TEC, not yet tested; Fig. 4C). Log-fold change values were plotted for docetaxel treated PC3 10 DPT vs docetaxel treated MDA-MB-231 10 DPT (Fig. 4D) and cisplatin treated PC3 10 DPT vs cisplatin treated MDA-MB-231 10 DPT (Fig. 4E). Within each treatment class, shared differentially expressed genes (DEGs) were positively correlated between MDA-MB-231 and PC3 cells, indicating the DEGs are upregulated to a similar magnitude.

Common transcription factors (TFs) and hallmark pathways upregulated in the survivors were delineated (Fig. 4F, G). Two significantly enriched TFs, ZNF697 and NPAS2, were previously reported in cells that transition out of senescence and into a proliferative state [27]. Top enriched hallmark pathways in the 309 gene survivor data set were: epithelial-to-mesenchymal transition (EMT), upregulation of KRAS signaling, coagulation, TNFα signaling via NFkB, and hypoxia (Fig. 4F). Single cell gene enrichment confirmed the top upregulated hallmark pathways in the shared survivor data set (Figs. 4H, S10-11). Additional pathways identified to be significantly upregulated in the surviving cells were: PI3K-AKT-mTOR signaling, inflammatory response, and cholesterol homeostasis (Figs. 4H, S10-11).

Identification of HOMER1, TNFRSF9, and LRP1 as putative chemotherapy RNA survival markers

Utilizing the shared cell survivor gene set data, markers were independently evaluated to understand their putative role in

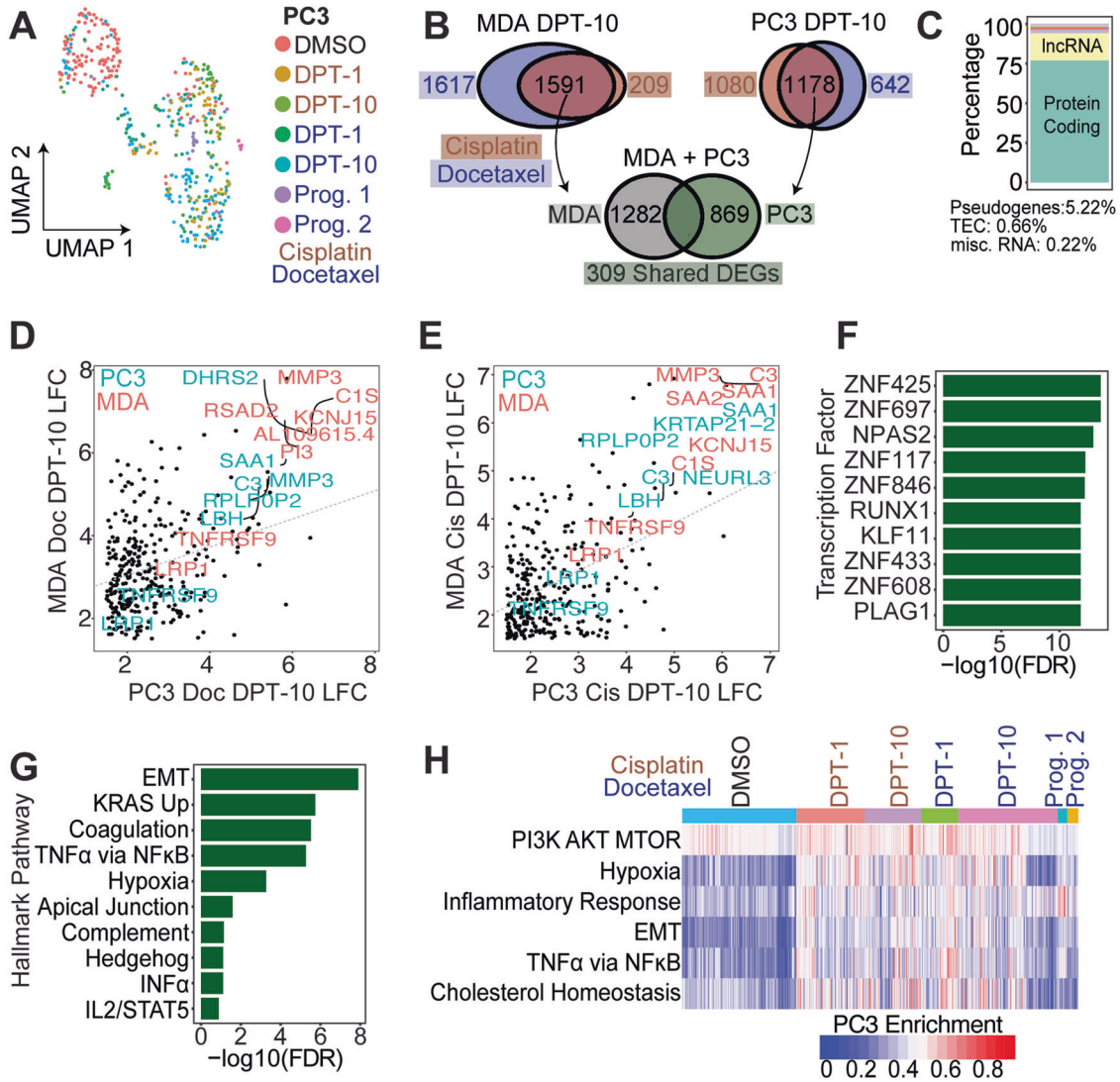

Fig. 4 Chemotherapy induced surviving tumor cells share common phenotypes and pathways for survival. A UMAP of all conditions for PC3 cells. **B** Venn diagram of upregulated DEGs between MDA-MB-231 10 DPT and PC3 10 DPT cells compared to respective controls. From the shared DEGs between cisplatin and docetaxel treatments, MDA-MB-231 and PC3 shared 309 upregulated genes compared to their respective controls. **C** Genecode annotations for the 309 shared genes. TEC: to be experimentally confirmed, not tested. log-fold change (LFC) of shared 309 genes for PC3 vs MDA-MB-231 for (**D**) docetaxel and (**E**) cisplatin treatments, respectively. **F** CHEA3 transcription factor enrichment of the shared 309 polyploid genes. **G** Hallmark enrichment analysis of 309 shared genes. **H** Single cell Hallmark gene set enrichment analysis for all PC3 cells through JASMINE gene set enrichment (see methods).

chemotherapy survival and polyploid state. All 309 genes were investigated via literature review and queried for terms in September 2023, including: large tumor cell, polyploid giant cancer cell, poly-aneuploid cancer cell, survival pathways, drug resistance, chemotherapy, and apoptosis. With prior knowledge that top upregulated genes (MMP-3, SAA1, and C3) functioned in the execution of apoptosis and clearance of apoptotic bodies (Fig. 4D, E), and that SAA1 and C3 were correlated with better PFS (Fig. S12), they were not considered novel survival markers. The 309 gene survivor cell enrichment data set was also intersected with genes in the top enriched pathways that modulate survival: TNFα via NFkB, PI3K-AKT, and mTOR signaling (Fig. 4G, H). We identified TNFRSF9 and LRP1 as survival biomarkers; these are known to function as cell surface receptors that enhance PI3K activity. This activity, in turn, stimulates AKT, thereby promoting cell survival (Figs. 4D, E, 5, S13A) [28–30]. Further, we identified HOMER1 as a PC3-specific survival marker (Fig. 5); HOMER1 plays a role in mTOR signaling and protection against apoptosis [31–34].

HOMER1, TNFRSF9, and LRP1 are protein markers of chemotherapy survival and are retained in docetaxel treated PC3 progeny

At the protein level, we found surviving PC3 and MDA-MB-231 cells post-chemotherapy treatment stained positive for HOMER1, TNFRSF9, and LRP1 (Fig. 5A, D). Image quantification revealed all PC3 conditions (except for progeny-1 cisplatin day 10 post-treatment release) were significantly upregulated compared to controls (Fig. 5A, C). Day 10 survivors showed the highest protein expression levels for each marker tested. Importantly, untreated PC3 progeny-1 displayed significantly higher expression in all three survival markers tested compared to parental DMSO control cells, suggesting these markers were retained following treatment (Fig. 5A, C). CD45 is typically utilized as a tumor cell exclusion marker that stains for white blood cells. At day 10 post-treatment release time points we noted a gain in CD45 protein expression that was retained in progeny cells in PC3 cells (Figs. 5A, S13C). MDA-MB-231 cells also showed a significant upregulation of expression for most markers tested, except HOMER1 for docetaxel

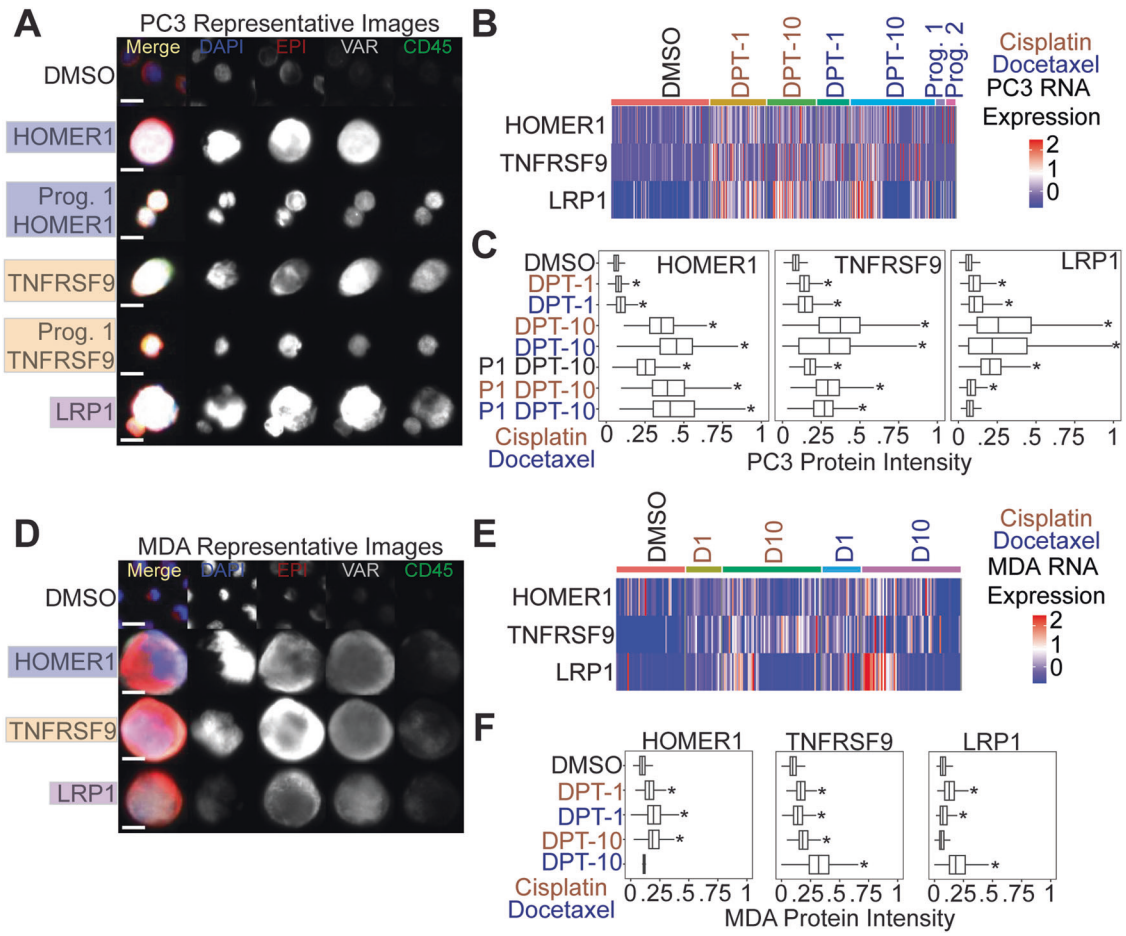

Fig. 5 HOMER1, TNFRSF9, and LRP1 are putative markers of chemotherapy resistance. A Representative PC3 images of putative marker genes stained in the variable (VAR) channel. DMSO control cells were stained with HOMER1 in the VAR channel. **B** RNA expression for each marker for all PC3 conditions. **C** Protein immunofluorescence quantification for PC3 cells stained with tested markers. **D** Representative MDA-MB-231 (MDA) images of putative marker genes stained in the VAR channel. DMSO control cells were stained with HOMER1. **E** RNA expression for each marker for all MDA-MB-231 cells. **F** Immunofluorescence quantification for MDA-MB-231 cells stained with tested markers. Wilcoxon rank sum test used in **C** and **F**; significance $p < 0.01$).

day 10 post-treatment release and LRP1 for cisplatin day 10 post-treatment release (Fig. 5D, F).

HOMER1, TNFRSF9, and LRP1 are found at the protein level patient bone marrow aspirate samples, and their increased expression is correlated with recurrence in public datasets

A subset of bone marrow samples that displayed a high frequency of CTC-IGC from the prostate cancer patient cohort (Fig. 1) were stained with HOMER1, TNFRSF9, and LRP1 (Fig. 6A). Patient 1 and patient 3 did not participate in the clinical trial but also displayed a high frequency of CTC-IGC (Table 1; see methods). All patients profiled had CTCs that were positive for the tested markers (Fig. 6B). While there were CTC-IGC positive for the marker genes in each patient sample (Fig. 6A), the tested markers were not selective for CTC-IGC (Fig. S14). Patient 5, who displayed the highest percentage of CTCs positive for markers HOMER1 and TNFRSF9, had the shortest PFS at 1.4 months (Fig. 6B, Table 1). Additionally, these survival markers identified cells in the bone marrow that displayed increased genomic content but were negative for canonical epithelial markers (Fig. S15).

In publicly available data for previously treated patients, high expression of TNFRSF9 and LRP1 significantly correlated with a shorter progression free survival in patients with prostate cancer; HOMER1 was not statistically significant (p-value = 0.183) (Fig. 6C). High gene expression of TNFRSF9, HOMER1, and LRP1 were all significantly correlated with worse relapse free survival in breast cancer (Fig. 6D). Taken together, we can conclude the survival genes are associated with recurrence at the RNA level and are present on CTCs-IGC in the bone marrow aspirate of late-stage prostate cancer patients.

DISCUSSION

Our analysis of bone marrow liquid biopsy samples from previously treated advanced prostate cancer patients reveals that the presence of polyploid cancer cells correlates with poorer progression-free survival. Although clinical reports have frequently observed polyploid cancer cells in later disease stages, a direct link with disease recurrence has not been firmly established. We also found that CTC-IGC have copy number profiles identical to typical CTCs and are predominantly present in the bone marrow rather than in peripheral blood.

Through single cell copy number profiling and the isolation of progeny from individual polyploid cells, we demonstrate that the polyploid cancer cell phenomenon represents a change in cell state.

Single-cell copy number profiling shows that the copy number ratios in patient CTC-IGC as well as chemotherapy induced polyploid MDA-MB-231 and PC3 cells that survive treatment are identical to those in their paired non-polyploid samples. This

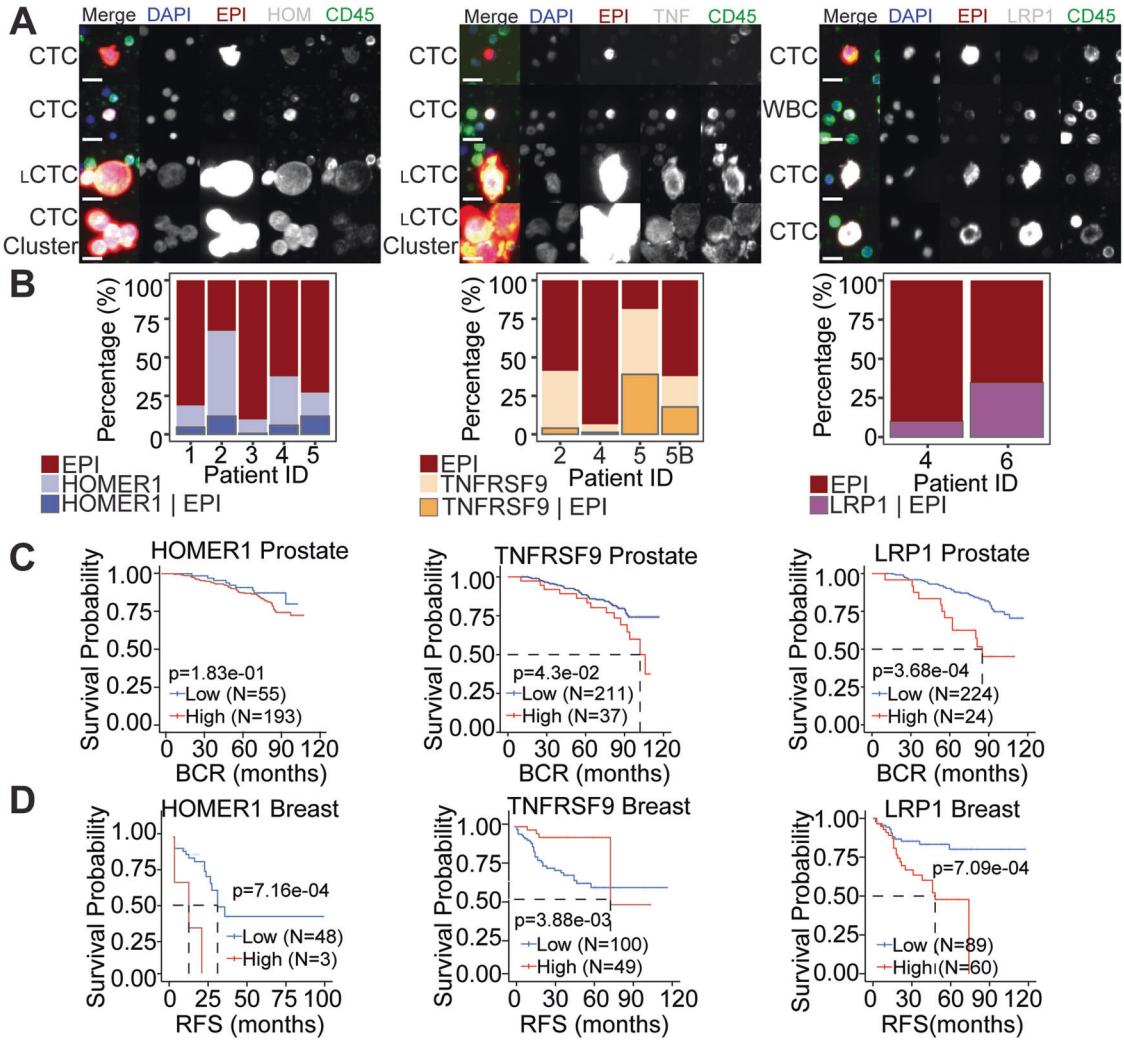

Fig. 6 HOMER1, TNFRSF9, and LRP1 are positive on CTCs in the bone marrow aspirate of late-stage prostate cancer and are correlated with recurrence in prostate and breast cancers. A Representative CTCs from bone marrow aspirate of advanced prostate cancer patients that were stained with survival markers HOMER1 (left), TNFRSF9 (TNF; middle), and LRP1 (right). Tested markers appear as white in the merged image. Scale bars are 15 μM. LCTC represent larger CTCs, or CTC-IGCs. **B** Percentages of rare cells with each channel positivity depicted. Cells were stained with survival markers HOMER1 (left), TNFRSF9 (middle), and LRP1 (right). Cells that have EPI positivity are tumor derived, while cells that are positive for the marker alone (middle bar in bar plot) cannot be conclusively labeled as a tumor derived cell. LRP1 (right) is also a marker of T-cells, so only cells that were EPI positive were included. Kaplan-Meyer survival plots for RNA expression of tested markers in prostate (**C**) and (**D**) breast cancer patients.

Table 1. PFS for patient bone marrow samples (in Fig. 6) that were stained for the putative survival markers TNFRSF9, LRP1, and HOMER1.

Patient ID	PFS
1	n.a.[a]
2	9.6
3	n.a.[a]
4	6.1
5	1.4
6	4.5

[a]not part of main trial & was not included.

indicates that these cells, either identified as patient CTCs or those that survive in the days following therapy release in vitro, undergo multiple rounds of WGD without any additional copy number alterations. These findings provide crucial insights into the dynamics and genetic stability of the polyploid cancer cell state.

Obtaining proliferative progeny proved challenging; after three months of culturing single isolated polyploid cells, we successfully derived only one proliferative progeny clone (1/1,440). This outcome is significant for two main reasons: first, it demonstrates that polyploid cancer cells can give rise to progeny, but second, the extremely low success rate underscores why these cells have historically been understudied. To enhance our understanding, future research should employ high-throughput techniques to isolate larger numbers of single cells, such as tens of thousands, which may prove critical in understanding the roles of non-proliferative polyploid cancer cells and assessing their capabilities at reinitiating cell division to give rise to progeny. Additionally, slight variations in the copy number profiles, such as a 3p gain observed in the progeny-1 clone, hint at genomic evolution. Further studies should explore this genomic evolution in different progeny clones once they are sufficiently collected to understand the dynamics of genomic re-organization in these cells.

Through in vitro single cell transcriptomics, we further provide evidence that polyploid cancer cells display a convergent phenotype between MDA-MB-231 (breast cancer) and PC3 (prostate cancer) model systems. Despite being induced with chemotherapies with contrasting mechanisms of action (cisplatin and docetaxel), the different tumor models displayed a shared polyploid signature of upregulating 309 common genes. This convergence reveals significant insights into the biological features of polyploid cancer cells.

In our observations, approximately 50% of polyploid cancer cells remained attached to the culture flask in a non-proliferative state during single cell progeny outgrowth experiments. Polyploid cancer cells have been identified to progress through the cell cycle but do not proliferate (i.e., endocycling or cytokinesis failure occur before mitosis) [35]. This is hypothesized to be a protective state of the cells that affords protection from therapeutic stressors. This phenomenon aligns with our identification of ZNF697 and NPAS2 as two transcription factors significantly enriched in the convergent polyploid gene set that were previously identified to be upregulated in cells that were in a non-proliferative state and began re-initiating cell division [27]. This suggests that some polyploid cells profiled on day 10 post therapy release may be attempting to re-initiate proliferation since the chemotherapy has been removed. This finding is further supported by a higher percentage of cells at 10 DPT expressing more markers at the M-phase of the cell cycle (Figs. S8-9). As polyploid cells attempt to re-initiate division, they express markers indicating resistance to or reversion from senescence (i.e., vimentin, ZNF697, NPAS2) however, many of these cells likely fail to reorganize their genomic content (e.g., progeny-2 erratic copy number profile), do not further proliferate, and ultimately die. Future research should explore the roles of ZNF697, NPAS2, and genomic reorganization in polyploid cancer cells and their implications for disease recurrence in progeny cells.

The convergent surviving cell gene set we identified indicated that pro-survival and anti-apoptotic pathways, such as TNFα via NFkB, PI3K-AKT, and mTOR signaling, are upregulated in polyploid cancer cells [36–38]. Among the genes identified in these pathways, TNFRSF9, HOMER1, and LRP1 were identified as putative survival genes and were found to be upregulated at the RNA and protein levels [28–34, 39–43]. Notably, these protein markers were retained in the PC3 progeny-1 clone, suggesting their upregulation in cells that survive chemotherapy. Additionally, a subset of CTCs, including both polyploid and typical CTCs, tested positive for TNFRSF9, HOMER1, and LRP1 at the protein level. Of note, Patient 5, who experienced the shortest progression-free survival at 1.4 months, had the highest percentage of CTCs positive for the TNFRSF9 marker, indicating that this gene may play a significant role in cancer cell survival. Further, these markers identified a subset of cells with IGC that were negative in the epithelial channel. These cells may be CTCs that lost epithelial expression (i.e., EMT) and, in combination with the upregulation of the proposed survival markers, could be adept at surviving in the bone marrow.

Interestingly, bulk gene expression studies from tumors found that HOMER1 was prognostic of worse PFS in breast cancer but not in prostate cancer, whereas cell line data suggested the opposite. This discrepancy may be addressed by evaluating additional cell line models for both prostate and breast cancer to understand if unique genomic or epigenetic factors (e.g., loss of promoter methylation) drive HOMER1 expression and contribute to therapy resistance. Ultimately, further studies are needed to evaluate the roles of TNFRSF9, HOMER1, and LRP1 in chemotherapy resistance and as a biomarker to evaluate the emergence of therapeutic resistance.

Our investigation of polyploid cancer cells confirms the significant upregulation of hypoxia and cholesterol homeostasis pathways. Studies have shown that targeting these pathways in cell line models, including PC3 and MDA-MB-231, reduces the viability of progeny from polyploid cancer cells [23, 26]. Further evidence comes from a study indicating that polyploid cancer cells accumulate lipid droplets in response to chemotherapy [44], underscoring the critical role of lipid balance as cells significantly increase in size. These findings suggest that these pathways are integral to the polyploid cancer cell state and represent promising targets for therapeutic intervention.

The in vitro environment of cell culture does not always recapitulate the in vivo nature of cancer cell biology. This makes it difficult to speculate how polyploid cancer cells interact with their neighboring malignant cells and the surrounding stroma. Translating the findings of TNFRSF9, HOMER1, and LRP1 as resistance markers in an in vivo model is a critical next step. Future studies should employ mouse models or patient derived xenografts and stain for these biomarkers to understand their prominence in vivo. Further studies should also isolate polyploid cancer cells through nuclear density to further understand their cellular phenotypes in tumor tissue.

While patient results are promising, they also have limitations. This study focuses on late-stage patients with disseminated CTCs in the bone marrow and blood. The evaluated cohort comprised advanced-stage patients whose previous treatment regimens had failed. To minimize biases associated with late-stage disease and to better understand initial treatment responses and their role in inducing polyploid cancer cells, future cohorts should include patients undergoing their first rounds of therapy. One concern is that CTCs in peripheral blood are typically found in later disease stages, potentially biasing our patient population towards later stages. Obtaining samples from tissue, blood, and bone marrow could address these concerns and provide valuable insights into the role of polyploid cancer cells in dissemination, initial response to therapy, and disease evolution.

METHODS

Patient sample collection and processing

Liquid biopsy samples were collected from clinical sites and processed at the University of Southern California as previously described [45, 46]. Briefly, peripheral blood and bone marrow aspirate samples were collected from patients immediately starting treatment on trial NCT01505868 that evaluated cabazitaxel with or without carboplatin in patients with metastatic castration-resistant prostate cancer. Samples were collected at MD Anderson Cancer Center prior to therapy.

Patients 1 and 3 did not participate in NCT01505868. Patient 1, a previous case study, was acquired from the Greater Los Angeles Veterans' Affairs Healthcare System [47]. The bone marrow sample was collected at the time of diagnostic biopsy, prior to treatment. Patient 3, another previous case study [48], was acquired from MD Anderson. All patients gave written informed consent in accordance with approved institutional review board and research development (VA) protocols.

Following isotonic erythrocyte lysis, the entire nucleated fraction was plated onto custom cell adhesion glass slides (Marienfield, Lauda, Germany) and stored at −80 °C until use [46].

Cell culture and drug treatment

PC3 and MDA-MB-231 cell lines were purchased from ATCC and grown in RPMI and DMEM, respectively, with 10% FBS and 0.5% penicillin/streptomycin. Cells were plated at a density of 625,000 cells per T-75 flask. Cells were treated with docetaxel (PC3: 5 nM, MDA-MB-221: 10 nM) or cisplatin (10 μM) for 72 hours. Cells were then allowed to recover in normal medium for 1 or 10 days. When indicated, cells were re-treated at day 10 post treatment removal. Cells were lifted from culture and plated on Marienfield glass slides for imaging or single cell isolation. All cell line experiments were conducted in triplicate.

To isolate progeny cells, PC3 cells 10 days post treatment were lifted with 1x versene. Biosorter (UnionBio, Holliston, MA) was used to sort single cells based on size and the largest 15% of cells were sorted into ten 96-well plates ($n = 960$ individual wells) containing RPMI medium and then placed in a 37 °C incubator. Media was changed every 2-3 days.

Immunofluorescent staining

Patient slides in Fig. 1 were fixed with paraformaldehyde and stained with a pan-cytokeratin cocktail mixture (see supplementary methods), conjugated mouse anti-human CD45 Alexa Fluor 647 (clone: F10-89-4, MCA87A647, AbD Serotec, Raleigh, NC, USA), Vimentin (Alexa Fluor 488 rabbit IgG monoclonal antibody (Cell Signaling Technology; Cat# 9854BC; Clone: D21H), and 4′,6-diamidino-2-phenylindole (DAPI; D1306, Thermo, Waltham, MA, USA) as previously described [46]. EpCAM (Thermo, 14-9326-82) was included in the pan-cytokeratin cocktail mixture to make an "EPI-cocktail".

TNFRSF9 (Thermo, PA5-98296) and HOMER1 (Thermo, PA5-21487) primary antibodies were incubated on slides overnight at 4 °C with the EPI-cocktail of antibodies. Slides were then washed and incubated at room temperature for two hours with Alexa Fluor 555 goat anti-mouse IgG1 antibody (Thermo, A21127), Alexa Fluor 488 goat anti-rabbit (Thermo, A11034), CD45, and DAPI.

LRP1 (Thermo, 377600) was generated in mice and was therefore not compatible with the EPI-cocktail. Instead, LRP1 was incubated overnight at 4 °C. Slides were then washed and incubated at room temperature for two hours with Alexa Fluor 555 goat anti-mouse IgG1 antibody. Next, pre-conjugated Alexa Fluor 488 pan-cytokeratin (53-9003-82, Thermo) recognizing CK 10, 14, 15, 16, and 19 was incubated with conjugated mouse anti-human CD45, and DAPI.

Slide imaging and analysis

Slides were imaged with an automated high throughput microscope equipped with a 10x optical lens, as previously described [45]. Immunofluorescent and bright field images were collected. Image analysis tool, available at https://github.com/aminnaghdloo/slide-image-utils, was developed in python using the OpenCV and scikit-image packages [49, 50]. Briefly, each fluorescent channel was segmented individually using adaptive thresholding and merged into one cell mask. Cell mask and DAPI mask were used to extract features and fluorescent intensity statistics of single cells and their nuclei, respectively. For nucleus size analysis, equivalent diameter was calculated from nucleus area, assuming a circular shape.

Fluorescence in situ Hybridization

Probes for centromeres of chromosomes 1 (CHR01-10-GR) and 10 (CHR10-10-GR) were purchased from Empire Genomics (Depew, New York) and the hybridization was carried out on Marienfeld glass slides per the manufacturer's instructions. Slides were then stained with DAPI and then imaged.

Single cell copy number profiling

Single cells were isolated as previously described [46]. Copy number profiling from low pass whole genome sequencing samples was conducted as previously described (see supplementary methods) [51, 52].

Single cell RNA sequencing

Single cells were isolated and picked via micro-manipulation as previously described. RNA was extracted via a modified Smart-Seq2 approach and library prepped with Nextera XT (Illumina, San Diego, CA). Cells were sequenced paired end by 150 base-pairs on an Illumina HiSeq 4000 (Fulgent). Read adapters were trimmed with TrimGalore (version 0.6.7) and aligned with the HiSat2 (v2.2.1). Picard (v3.0.0) was used to visualize RNA mapping quality control [53–55]. HTSeq (v2.0.2) was used to generate a gene count matrix [56].

Downstream analysis was performed with R (v4.1.2). The SingleCellExperiment package (v4.2.2) was utilized for inputting count data into downstream analyses, such as converting to Seurat (v4.3.0) and edgeR (v3.36.0) count matrices [57]. Data visualization was performed with Seurat and ggplot2 (v3.4.4), and Pheatmap (v1.0.12) packages.

The edgeRQLFDetRate differential expression pipeline was used to find common upregulated genes in polyploid cancer cells [58]. Sequencing batches were controlled for. Shared genes expressed in surviving large cells were intersected through R.

Gene datasets were downloaded directly from CHEA3 [59] and MSigDB [60] for transcription factor and hallmark pathway enrichment, respectively. Single cell enrichment was conducted through JASMINE [61].

Survival analysis

Survival analysis from patient bone marrow and peripheral blood samples was performed with the Survival R package (v3.5.5) and plotted with ggplot2 (v3.4.4). Public gene expression survival analysis was analyzed via PanCancSurvPlot [62] for prostate cancer (GSE116918) and breast cancer (GSE10893) [63, 64].

DATA AVAILABILITY

Cell line scDNA-seq (GSE270567) and scRNA-seq (GSE270568) are available through GEO. Patient scDNA-seq is available upon reasonable request. Image data is available upon reasonable request for cell lines and patients. If interested in using the High Definition Single Cell Assay please contact CSI-Cancer.

CODE AVAILABILITY

Image analysis code is freely available at https://github.com/aminnaghdloo/slide-image-utils. Downstream analysis scripts (DNA-seq, RNA-seq, image quantification) are available upon request.

REFERENCES

1. Kurbegovic S, Berg KD, Thomsen FB, Gruschy L, Iversen P, Brasso K, et al. The risk of biochemical recurrence for intermediate-risk prostate cancer after radical prostatectomy. Scand J Urol. 2017;51:450–6.
2. Goss PE, Ingle JN, Pritchard KI, Robert NJ, Muss H, Gralow J, et al. Extending aromatase-inhibitor adjuvant therapy to 10 years. N. Engl J Med. 2016;375:209–19.
3. Colleoni M, Sun Z, Price KN, Karlsson P, Forbes JF, Thurlimann B, et al. Annual hazard rates of recurrence for breast cancer during 24 years of followup: Results from the international breast cancer study group trials i to v. J Clin Oncol. 2016;34:927–35.
4. Bukowski K, Kciuk M, Kontek R. Mechanisms of multidrug resistance in cancer chemotherapy. Int J Mol Sci. 2020;21:3233.
5. Ashdown ML, Robinson AP, Yatomi-Clarke SL, Ashdown ML, Allison A, Abbott D, et al. Chemotherapy for late-stage cancer patients: Meta-analysis of complete response rates. F1000Res. 2015;4:232.
6. Wang X, Zhang H, Chen X. Drug resistance and combating drug resistance in cancer. Cancer Drug Resist. 2019;2:141–60.
7. Cree IA, Charlton P. Molecular chess? hallmarks of anti-cancer drug resistance. BMC Cancer. 2017;17:10.
8. Siegel RL, Miller KD, Wagle NS, Jemal A. Cancer statistics, 2023. CA Cancer J Clin. 2023;73:17–48.
9. Trabzonlu L, Pienta KJ, Trock BJ, De Marzo AM, Amend SR. Presence of cells in the polyaneuploid cancer cell (pacc) state predicts the risk of recurrence in prostate cancer. Prostate. 2023;83:277–85.
10. Fei F, Zhang D, Yang Z, Wang S, Wang X, Wu Z, et al. The number of polyploid giant cancer cells and epithelial-mesenchymal transition-related proteins are associated with invasion and metastasis in human breast cancer. J Exp Clin Cancer Res. 2015;34:158.
11. Amend SR, Torga G, Lin K-C, Kostecka LG, Marzo A, Austin RH, et al. Polyploid giant cancer cells: Unrecognized actuators of tumorigenesis, metastasis, and resistance. Prostate. 2019;79:1489–97.
12. Lopez-Sanchez LM, Jimenez C, Valverde A, Hernandez V, Penarando J, Martinez A, et al. Cocl2, a mimic of hypoxia, induces formation of polyploid giant cells with stem characteristics in colon cancer. PLoS One. 2014;9:99143.
13. Was H, Borkowska A, Olszewska A, Klemba A, Marciniak M, Synowiec A, et al. Polyploidy formation in cancer cells: How a trojan horse is born. Semin Cancer Biol. 2022;81:24–36.
14. Saleh T, Carpenter VJ, Bloukh S, Gewirtz DA. Targeting tumor cell senescence and polyploidy as potential therapeutic strategies. Semin Cancer Biol. 2022;81:37–47.
15. Ogden A, Rida PCG, Knudsen BS, Kucuk O, Aneja R. Docetaxel-induced polyploidization may underlie chemoresistance and disease relapse. Cancer Lett. 2015;367:89–92.
16. Puig P-E, Guilly M-N, Bouchot A, Droin N, Cathelin D, Bouyer F, et al. Tumor cells can escape dna-damaging cisplatin through dna endoreduplication and reversible polyploidy. Cell Biol Int. 2008;32:103–43.
17. Adibi R, Moein S, Gheisari Y. Zoledronic acid targets chemo-resistant polyploid giant cancer cells. Sci Rep. 2023;13:419.
18. Bielski CM, Zehir A, Penson AV, Donoghue MTA, Chatila W, Armenia J, et al. Genome doubling shapes the evolution and prognosis of advanced cancers. Nat Genet. 2018;50:1189–95.
19. Lopez S, Lim EL, Horswell S, Haase K, Huebner A, Dietzen M, et al. Interplay between whole-genome doubling and the accumulation of deleterious alterations in cancer evolution. Nat Genet. 2020;52:283–93.
20. Pienta KJ, Hammarlund EU, Austin RH, Axelrod R, Brown JS, Amend SR. Cancer cells employ an evolutionarily conserved polyploidization program to resist therapy. Semin Cancer Biol. 2022;81:145–59.

21. Pienta KJ, Hammarlund EU, Axelrod R, Brown JS, Amend SR. Polyaneuploid cancer cells promote evolvability, generating lethal cancer. Evol Appl. 2020;13:1626–34.
22. Zhou X, Zhou M, Zheng M, Tian S, Yang X, Ning Y, et al. Polyploid giant cancer cells and cancer progression. Front Cell Dev Biol. 2022;10:1017588.
23. White-Gilbertson S, Lu P, Esobi I, Echesabal-Chen J, Mulholland PJ, Gooz M, et al. Polyploid giant cancer cells are dependent on cholesterol for progeny formation through amitotic division. Sci Rep. 2022;12:8971.
24. Zhou M, Ma Y, Chiang C-C, Rock EC, Butler SC, Anne R, et al. Single cell morphological and transcriptome analysis unveil inhibitors of polyploid giant breast cancer cells in vitro. Commun Biol. 2023;6:1301.
25. Zhang X, Yao J, Li X, Niu N, Liu Y, Hajek RA, et al. Targeting polyploid giant cancer cells potentiates a therapeutic response and overcomes resistance to parp inhibitors in ovarian cancer. Sci Adv. 2023;9:7195.
26. Carroll C, Manaprasertsak A, Bo elli, Castro A, Bos H, Spierings DC, et al. Drug resilient cancer cell phenotype is acquired via polyploidization associated with early stress response coupled to hif2 transcriptional regulation. Cancer Res Commun. 2024;4:691–705.
27. Martinez-Zamudio RI, Stefa A, Nabuco Leva Ferreira Freitas JA, Vasilopoulos T, Simpson M, Dor EG, et al. Escape from oncogene-induced senescence is controlled by pou2f2 and memorized by chromatin scars. Cell Genom. 2023;3:100293.
28. So T, Croft M. Regulation of pi-3-kinase and akt signaling in t lymphocytes and other cells by tnfr family molecules. Front Immunol. 2013;4:139.
29. Luo L, Wall AA, Tong SJ, Hung Y, Xiao Z, Tarique AA, et al. Tlr crosstalk activates lrp1 to recruit rab8a and pi3ky for suppression of inflammatory responses. Cell Rep. 2018;24:3033–44.
30. He Z, Wang G, Wu J, Tang Z, Luo M. The molecular mechanism of lrp1 in physiological vascular homeostasis and signal transduction pathways. Biomedicine Pharmacother. 2021;139:111667.
31. Fei F, Li J, Rao W, Liu W, Chen X, Su N, et al. Upregulation of homer1a promoted retinal ganglion cell survival after retinal ischemia and reperfusion via interacting with erk pathway. Cell Mol Neurobiol. 2015;35:1039–48.
32. Luo P, Zhao Y, Li D, Chen T, Li S, Chao X, et al. Protective effect of homer 1a on tumor necrosis factor-alpha with cycloheximide-induced apoptosis is mediated by mitogen-activated protein kinase pathways. Apoptosis. 2012;17:975–88.
33. Lv W, Zhang Q, Li Y, Liu D, Wu X, He X, et al. Homer1 ameliorates ischemic stroke by inhibiting necroptosis-induced neuronal damage and neuroinflammation. Inflamm Res. 2024;73:131–44.
34. Reshetnikov VV, Bondar NP. The role of stress-induced changes of homer1 expression in stress susceptibility. Biochemistry. 2021;86:613–26.
35. Kim C-J, Gonye AL, Truskowski K, Lee C-F, Cho Y-K, Austin RH, et al. Nuclear morphology predicts cell survival to cisplatin chemotherapy. Neoplasia. 2023;42:100906.
36. Bhaskar PT, Hay N. The two torcs and akt. Dev Cell. 2007;12:487–502.
37. Sharma S, Yao H-P, Zhou Y-Q, Zhou J, Zhang R, Wang M-H. Prevention of bms-777607-induced polyploidy/senescence by mtor inhibitor azd8055 sensitizes breast cancer cells to cytotoxic chemotherapeutics. Mol Oncol. 2014;8:469–82.
38. You B, Xia T, Gu M, Zhang Z, Zhang Q, Shen J, et al. Ampk-mtor-mediated activation of autophagy promotes formation of dormant polyploid giant cancer cells. Cancer Res. 2022;82:846–58.
39. Smith SF, Collins SE, Charest PG. Ras, pi3k and mtorc2 - three's a crowd? J Cell Sci 133 (2020)
40. Dan HC, Antonia RJ, Baldwin AS. Pi3k/akt promotes feedforward mtorc2 activation through ikk-alpha. Oncotarget. 2016;7:21064–75.
41. Gaur U, Aggarwal BB. Regulation of proliferation, survival and apoptosis by members of the tnf superfamily. Biochem Pharm. 2003;66:14038.
42. Gonias SL, Campana WM. Ldl receptor-related protein-1: a regulator of inflammation in atherosclerosis, cancer, and injury to the nervous system. Am J Pathol. 2014;184:18–27.
43. Terrand J, Bruban V, Zhou L, Gong W, El Asmar Z, May P, et al. Lrp1 controls intracellular cholesterol storage and fatty acid synthesis through modulation of wnt signaling. J Biol Chem. 2009;284:381–8.
44. Kostecka LG, Pienta KJ, Amend SR. Lipid droplet evolution gives insight into polyaneuploid cancer cell lipid droplet functions. Med Oncol. 2021;38:133.
45. Marrinucci D, Bethel K, Kolatkar A, Luttgen MS, Malchiodi M, Baehring F, et al. Fluid biopsy in patients with metastatic prostate, pancreatic and breast cancers. Phys Biol. 2012;9:016003.
46. Chai S, Matsumoto N, Storgard R, Peng C-C, Aparicio A, Ormseth B, et al. Platelet-coated circulating tumor cells are a predictive biomarker in patients with metastatic castrate-resistant prostate cancer. Mol Cancer Res. 2021;19:2036–45.
47. Malihi PD, Morikado M, Welter L, Liu ST, Miller ET, Cadaneanu RM, et al. Clonal diversity revealed by morphoproteomic and copy number pro les of single prostate cancer cells at diagnosis. Converg Sci Phys Oncol. 2018;4:015003. https://doi.org/10.1088/2057-1739/aaa00b.
48. Chai S, Ruiz-Velasco C, Naghdloo A, Pore M, Singh M, Matsumoto N, et al. Identification of epithelial and mesenchymal circulating tumor cells in clonal lineage of an aggressive prostate cancer case. NPJ Precis Oncol. 2022;6:41.
49. Itseez: Open Source Computer Vision Library. https://github.com/itseez/opencv (2015).
50. Walt S, Schonberger JL, Nunez-Iglesias J, Boulogne F, Warner JD, Yager N, et al. contributors: scikit-image: image processing in python. PeerJ. 2014;2:453. https://doi.org/10.7717/peerj.453.
51. Baslan T, Kendall J, Ward B, Cox H, Leotta A, Rodgers L, et al. Optimizing sparse sequencing of single cells for highly multiplex copy number profling. Genome Res. 2015;25:714–24.
52. Schmidt, MJ, Prabakar, RK, Pike, S, Yellapantula, V, Peng, C-C, Kuhn, P, et al. Simultaneous copy number alteration and single-nucleotide variation analysis in matched aqueous humor and tumor samples in children with retinoblastoma. Int J Mol Sci. 2023;24:8606–19.
53. Krueger, F, James, F, Ewels, P, Afyounian, E, Weinstein, M, Schuster-Boeckler, B, et al., sclamons: FelixKrueger/TrimGalore: v0.6.10 (0.6.10). Zenodo (2023)
54. Kim D, Paggi JM, Park C, Bennett C, Salzberg FP. Graph-based genome alignment and genotyping with hisat2 and hisat-genotype. Nat Biotechnol. 2019;37:907–15. https://doi.org/10.1038/s41587-019-0201-4.
55. Institute, B: Picard. https://broadinstitute.github.io/picard/.
56. Anders S, Pyl PT, Huber W. Htseq – a python framework to work with high throughput sequencing data. bioinformatics. 2015;31:166–9.
57. Amezquita RA, Lun ATL, Becht E, Carey VJ, Carpp LN, Geistlinger L, et al. Orchestrating single-cell analysis with bioconductor. Nat Methods. 2020;17:137–45.
58. Soneson C, Robinson MD. Bias, robustness and scalability in single-cell differential expression analysis. Nat Methods. 2018;15:255–61.
59. Keenan AB, Torre D, Lachmann A, Leong AK, Wojciechowicz ML, Utti V, et al. Chea3: transcription factor enrichment analysis by orthogonal omics integration. Nucleic Acids Res. 2019;47:212–24.
60. Liberzon A, Birger C, Thorvaldsd ottir H, Ghandi M, Mesirov JP, Tamayo P. The molecular signatures database (msigdb) hallmark gene set collection. Cell Syst. 2015;1:417–25.
61. Noureen, N, Ye, Z, Chen, Y, Wang, X, Zheng, S. Signature-scoring methods developed for bulk samples are not adequate for cancer single-cell rna sequencing data. Elife 2022;11:71994–206.
62. Lin, A, Yang, H, Shi, Y, Cheng, Q, Liu, Z, Zhang, J, et al.: Pancansurvplot: A large-scale pan-cancer survival analysis web application. bioRxiv (2022)
63. Jain S, Lyons CA, Walker SM, McQuaid S, Hynes SO, Mitchell DM, et al. Validation of a metastatic assay using biopsies to improve risk stratification in patients with prostate cancer treated with radical radiation therapy. Ann Oncol. 2018;29:215–22.
64. Weigman VJ, Chao H-H, Shabalin AA, He X, Parker JS, Nordgard SH, et al. Basal-like breast cancer dna copy number losses identify genes involved in genomic instability, response to therapy, and patient survival. Breast Cancer Res Treat. 2012;133:865–80.

ACKNOWLEDGEMENTS

We would like to thank the patients and their caretakers, including those on active duty and veterans, for participating in this study, without whom this research would not have been possible. We thank the clinical and research consent teams MDAnderson and the VA clinics for supporting the enrollment of patients and sample collections. Components of Fig. 2 was created using Biorender.com.

AUTHOR CONTRIBUTIONS

Conceptualization: MJS, RKP, KJP, SRA, and JH; Methodology: MJS, AN, RKP; Software: MJS, AN; Formal analysis: MJS; Investigation: MJS and MK; Resources: PK and JH; Writing—Original Draft: MJS, JH, and SRA; Writing—Review and Editing: MJS, SRA, RKP, ML, MK, AN, KJP, PK, AA, AZ-W, PC; Visualization: MJS; Supervision: KJP, SRA, JH; Project Administration: KJP, SRA, JH; Funding Acquisition: PK, KJP, SRA, JH, ML; Patient Accrual: ML, RC, IPG, AA, AZ-W, PC.

FUNDING

This work was funded in whole or in part by Epic Sciences (PK, JH), NCI P01CA093900 (PK, JH), and the NCI's USC Norris Comprehensive Cancer Center (CORE) Support 5P30CA014089-40 (PK, JH). SRA is supported by the US Department of Defense CDMRP/PCRP (W81XWH-20-10353, W81XWH-22–1-0680), the Patrick C. Walsh Prostate Cancer Research Fund and the Prostate Cancer Foundation. KJP is supported by NCI grants PO1CA093900, U54CA210173, U01CA196390, and P50CA058236, and the Prostate Cancer Foundation. PC receives funding from Janssen. Open access funding provided by SCELC, Statewide California Electronic Library Consortium.

COMPETING INTERESTS

The HDSCA technology described here is licensed to Epic Sciences. PK has ownership in Epic Sciences. JH discloses he is a member of the Clinical Advisory Board of Epic

Sciences. KJP is a consultant for CUE Biopharma, Inc., and holds equity interest in CUE Biopharma, Inc., Keystone Biopharma, Inc., PEEL Therapeutics, Inc and Kreftect, Inc. SRA holds equity interest in Keystone Biopharma, Inc.

ETHICS APPROVAL AND CONSENT TO PARTICIPATE

The study was conducted according to the guidelines of the Declaration of Helsinki and approved by the Institutional Review Board of the University of Southern California Keck School of Medicine, MD Anderson (NCT01505868), and the VA of Los Angeles (PCC 2015-090980). Informed consent was obtained from all subjects involved in the study.

CONSENT FOR PUBLICATION

All the authors agree to publish this paper.

ADDITIONAL INFORMATION

Supplementary information The online version contains supplementary material available at https://doi.org/10.1038/s41388-024-03212-z.

Correspondence and requests for materials should be addressed to Sarah R. Amend or James Hicks.